Science World Journal Vol. 20(No 3) 2025 https://dx.doi.org/10.4314/swj.v20i3.9
www.scienceworldjournal.org
ISSN: 1597-6343 (Online), ISSN: 2756-391X (Print)
Published by Faculty of Science, Kaduna State University

Full Length Research Article

EFFECT OF INCLINED ANGLE ON AIR BODY FORCE DURING AIR FLOW PROCESS INDUCED IN A RECTANGULAR BUILDING

*[1]A.S. Yakasai, [1]U. Sani, [1]B.G. Agaie, [2]A.L. Muhammad

[1]Department of Mathematics, Federal University Dutse, Jigawa State, Nigeria
[2]Kano State University of Science and Technology, Wudil, Kano State, Nigeria

*Corresponding Author Email Address: abbayakasai@yahoo.com

ABSTRACT
This study investigates the effect of inclined airflow angles on the air body force and its influence on buoyancy-driven ventilation in an un-stratified cross-ventilated rectangular domain with three openings. The airflow is primarily driven by the stack effect, where temperature differences between indoor and outdoor create density gradients, resulting in natural convection with an opposing flow introduced through one of the upper openings to mimic realistic ventilation input. The study focuses on three inlet airflow angles: 30°, 45°, and 55°, to assess their impact on temperature and velocity distribution within the domain. The system is modeled using a single-zone, one-dimensional approach, governed by steady-state Navier–Stokes equations. The equations are expressed in dimensionless form and solved using analytical method for ordinary differential equations (ODEs) to derive explicit solutions. Results show that lower airflow angles (e.g., 30°) enhance airflow momentum along the primary flow directions, intensifying convection and promoting faster air exchange, while higher angles (e.g., 55°) reduce airflow efficiency and flatten temperature gradients. The analysis also reveals that effective thermal coefficient impacts buoyancy force magnitude, altering the flow dynamics, and Prandtl number affects how fast heat moves compared to velocity, influencing stratification and mixing. The findings provide insight into optimizing natural ventilation design in buildings and support the development of energy-efficient, passive cooling strategies in architectural and engineering applications.

Keywords: Inclined Angle, Cross Ventilation, Rectangular Domain, Temperature Differences, and Velocity Distribution.

INTRODUCTION

Airflow within enclosures such as buildings, ducts, or natural ventilation systems is a key area of research in thermal-fluid sciences. Understanding how air moves under the influence of temperature gradients and external forces (like inclination or gravity) is fundamental to improving the design and efficiency of heating, ventilation, and air conditioning (HVAC) systems, passive cooling systems, and various environmental controls in both industrial and domestic settings.

Natural convection flows in rectangular enclosures, particularly when influenced by inclined angles, have been the subject of increasing attention due to their wide applications in solar collectors, electronic cooling systems, building thermal insulation, and energy-efficient architecture. The inclination of a cavity can significantly alter the characteristics of buoyancy-driven flow and heat transfer, thereby affecting thermal performance and comfort conditions within a space. One of the essential challenges in fluid dynamics is to analyze and predict how varying the inclination angle affects the air body force during flow in a cavity. This effect becomes more critical when dealing with stratified or thermally layered flow systems, where the alignment of thermal gradients relative to gravity can significantly enhance or suppress convective motions.

The significance of this investigation lies in its potential contribution to optimizing thermal systems and improving energy efficiency in built environments. By focusing on the influence of the inclined angle on the air body force during the airflow process in a rectangular building model, the study addresses a practical problem with real-world relevance to architecture, HVAC system design, and thermal comfort and offers valuable contributions in improving understanding of inclined natural convection, application in sustainable building design and enhanced indoor air quality and thermal comfort. Some researchers have made an effort to investigate this phenomenon: (Emswiler, 1926) investigated the case of multiple openings in a wall and obtained an expression for the rate of flow of air in terms of temperature differences using Bernoulli's Equation for ideal flow, and they did not consider the case of a single opening. The study of natural convection has been extensively focused on air flow issues in buildings, with practical applications ranging from heating equipment to turbine blade cooling. In translating the condition of this experiment to a sitting room of about ten times greater linear dimensions, it's found that the difference in density of CO_2 at the dimensions of the model corresponds to a temperature difference of about $10°C$ of the air inside and outside the sitting room by (Schmidt, 1961). (Linden *et al*., 1990) described the fluid mechanics of the natural ventilation of a space connected to a large body of stationary ambient fluid. The flows are driven by buoyancy differences between the interior and exterior fluids, connections with the ambient fluid are high level and low-level openings. Two forms of ventilation are identified: mixing ventilation and displacement ventilation. (Yuguo and Heiselberg, 2000) considered building having two openings at different vertical level on opposite walls, the height of the two openings is relatively small, and the areas of the top and bottom openings are A_t and A_b respectively. There is an indoor source of heat E, the wind force can assist or oppose the thermal buoyancy force, when the indoor temperature is uniform and specified the ventilation flow rate driven by stack force alone. (Yuguo *et al.,* 2000) presented a consistent pressure-based formulation for natural ventilation of single-zone and multi-zone buildings with multiple openings. A new analytical solution is presented for evaluating multi-zone airflow programs. It is found that wind force plays a vital role in natural ventilation design for this kind of buildings. A higher height of Zone 2, e.g. an atrium, cannot always increase the ventilation rate in zones. (Camille *et al*., 2003) considered single-sided natural ventilation, by using a computational fluid dynamics (CFD) model, together with analytical and empirical models. The CFD model was applied to determine the effects of buoyancy, wind, or their combination on

Science World Journal Vol. 20(No 3) 2025 https://dx.doi.org/10.4314/swj.v20i3.9
www.scienceworldjournal.org
ISSN: 1597-6343 (Online), ISSN: 2756-391X (Print)
Published by Faculty of Science, Kaduna State University

ventilation rates and indoor conditions. This investigation found CFD tools to be valid for studying single-sided natural ventilation strategies with respect to indoor, outdoor, and combined indoor and outdoor flow. (Yang, 2004) considered natural ventilation in a full-scale building induced by combined wind and buoyancy forces. A steady envelope flow model was applied to calculate mean ventilation rates. CFD model for the naturally ventilated buildings verified and validated. (Mostafa and Imam, 2009) studied the combination of natural ventilation methods in a single-sided room with a vertical vent. They evaluated ventilation rate through openings using air flow velocity measurements. The results clarified the effects of the vent on ventilation rate and suggested a model for the combination of both methods. Pressure measurements and PIV measurements were conducted in a detached house model with two openings. (Chow, 2010) described Air flow rate across a vertical opening induced by a thermal source in a room, various parameters were used in designing natural ventilation. Analytical expressions derived from simple hydraulic model were reviewed. (Sui *et al.,* 2011) used computational fluid dynamics (CFD) to simulate thermal natural ventilation in a civil building. They analyzed the natural ventilation rate, temperature difference, and thermal stratification height trends in different conditions. The simulation results can provide a theoretical foundation for designing natural ventilation systems. (Chaofan and Noor, 2012) proposed a new ventilation method for aircraft cabins using a square-wave periodic airflow instead of traditional steady airflow. The periodic inlet causes the air jet to oscillate, which improves mixing between fresh and cabin air, potentially enhancing ventilation performance without increasing airflow rate. Simulation results suggest better air distribution, but further real-world testing is recommended to confirm these findings. (Jianjun and Karava, 2014) described a model predictive control (MPC) strategy for buildings with mixed-mode cooling (window opening position, fan assist, and night cooling schedule) and demonstrates their potential performance bounds in terms of energy savings within thermal comfort constraints, in comparison with standard heuristic rules used in current practice. The study examined the air flow process across vertical vents induced by a stack-driven effect with an opposing flow in one of the upper openings. Some parameters and factors such as, area, height, size and position of the openings are described. Analytical techniques were employed and obtained the possible solutions of effective velocity distribution, effective temperature distribution, volumetric airflow and mass transfer rates. The orientation of the domain has a strong effect to the airflow around it, the temperature distributions and induced natural airflow rate depend highly on area of the openings by (Muhammad and Baffa, 2015). (Attalla *et al.,* 2017) investigates the impact of inlet airflow angle on airflow, temperature, and CO2 concentration in a three-row airliner cabin. It uses Ansys-Fluent and compares results with experimental data. Results show that changing the inlet airflow angle significantly improves flow pattern, temperature distributions, and CO_2 levels. Small inlet angles enhance the performance of the mixing-air distribution system. Angles B (5°) and C (10°) provide the best ventilation performance. (Jie *et al.*, 2024) proposes a realistic method to estimate natural ventilation potential in urban buildings by considering climate, wind patterns, and air pollution. Using CFD simulations and real-time data, it shows that traditional design estimates often overstate potential. Factors like heatwaves, poor air quality, and urban layout can significantly reduce actual ventilation performance. The framework helps guide more accurate and energy-efficient building designs. (Mo, 2024) investigated the mechanism by which the spray angle and airflow speed influence the dust reduction effect and reproduce a spray dust reduction process in a simulation. Based on the DPM (discrete phase model) and the mixture model, a spray dust reduction evaluation model was constructed by considering two-way momentum coupling between the discrete phase and the continuous phase. The results showed that installing nozzles near the dust source (coal mining drum) significantly reduced the dust concentration at the coal mining face from 0.0005 kg/m3 to 0.0001 kg/m3. And when the spray angle is 45◦, increasing the airflow speed provides a better dust reduction effect. (Hao *et al.*, 2025) examines how different roof styles affect natural ventilation and passive cooling in courtyard buildings. While previous research mainly focused on external conditions, this study highlights the importance of airflow between indoor spaces and courtyards. Using CFD simulations validated by wind tunnel experiments, the study compares various roof types, including flat, dome, butterfly, and shed roofs. Results show that roof geometry strongly influences airflow and indoor temperature. The dome roof performed best, increasing indoor wind speed by 80% and reducing temperatures by 2.1 °C, while the parapet roof performed the worst. The findings emphasize that not all courtyard designs are equally effective, with dome and shed roofs being optimal for natural ventilation.

Based on all the reviewed work mentioned above no body investigated the effect of the inclined angle on the air body force during the airflow process within a rectangular building which is the basis for this work. This research addresses a critical gap in the understanding of inclined natural convection by systematically analyzing how changes in the inclination angle influence airflow characteristics. The study aims to uncover the governing mechanisms that shape thermal and fluid behavior in inclined rectangular enclosures, ultimately contributing to more efficient, sustainable, and resilient thermal systems.

MATERIALS AND METHODS

The system represents a rectangular building with three openings. Two equal upper openings on opposite vertical walls with One lower opening on a vertical wall. The domain is cross-ventilated and considered unstratified. The vertical rectangular openings separating the domain have a height y^* and width x_w, the air acts as the connecting fluid, with properties: Density ρ, Temperature T, Pressure p and Inclined angle θ. The air enters through the lower opening and exits through one of the upper openings, while the other upper opening experiences an opposing flow with an indirect velocity v_0. The temperature difference induces natural convection, influencing the airflow.

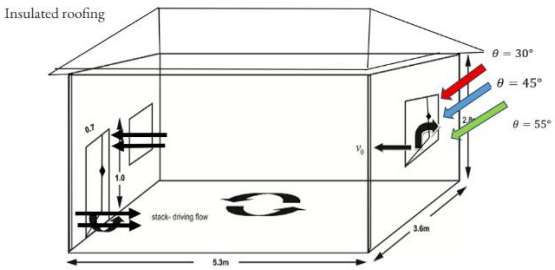

Figure 1: Schematic diagram of Cross section of a typical un-stratified cross- ventilated rectangular domain with three openings showing the effect of inclined angle on air body force.

Science World Journal Vol. 20(No 3) 2025 https://dx.doi.org/10.4314/swj.v20i3.9
www.scienceworldjournal.org
ISSN: 1597-6343 (Online), ISSN: 2756-391X (Print)
Published by Faculty of Science, Kaduna State University

Temperature differences between the indoor (T_i) and outdoor (T_o) of a domain produce density differences and corresponding pressure differences that generate buoyancy- driven flow through the domain envelope. The pressures gradient is a function of the constant width of the openings.

Momentum and Energy Equations with appropriate boundary conditions defined the problem. The model equations are represented in a dimensionless form and solved using the method of analytical techniques of solving ODEs using differential operators and boundary conditions to achieve explicit solutions. Convective motion induced by temperature differences effect as illustrated in Figure 1 is described, considering the inclined angle at which air enter the building by air body force of the fluid on momentum equation given by (Muhammad and Baffa 2015) the non- dimensionless equation become;

$$v_0 \frac{du}{dy} = g\beta\Delta T cos\theta + v\frac{d^2u}{dy^2} \quad (1)$$

$$v_0 \frac{dT}{dy} = \alpha \frac{d^2T}{dy^2} \quad (2)$$

Non-dimensional variables

Using the given transformations:

Length Scale: $y = y^*L$

Velocity Scale: $u = \frac{u^* g\beta\Delta T L^2}{\alpha}$

Reference Velocity: $v_0 = \frac{v_0^* \vartheta}{L}$

Temperature Scale: T = $T^*[\Delta T] + T^*{}_0$

Where y^*, u^*, v_0^*, T^* are dimensionless variables, corresponding to dimensional quantities $y(m)$, u and $v_0(m/s)$, and $T(k)$, respectively.

RESULTS AND DISCUSSION

To transform equation (1) and (2) into dimensionless equations, we use the given dimensionless variables above and get;

$$Pr\frac{d^2u^*}{dy^{*2}} + k\frac{du^*}{dy^*} + T^* cos\theta = 0 \quad (3)$$

$$\frac{d^2T^*}{dy^{*2}} + k\frac{dT^*}{dy^*} = 0 \quad (4)$$

by letting $k = -Prv_0$.

the dimensionless boundary conditions are;

$$0 \le y^* \le 1, u^*(y^* = 0) = 0, u^*(y^* = 1) = 0, T^*(y^* = 0) = -T^*{}_0, T^*(y^* = 1) = 1 - T^*{}_0.$$

the dimensionless group $Pr = \frac{\nu}{\alpha}$ is called Prandtl number, $u^*(y^*), T^*(y^*)$ is the velocity, and temperature distributions of the air, y^* is the dimensionless height of the openings.

Temperature Distribution

$$T^*(y^*) = c_1 + c_2 e^{-ky^*} \quad (5)$$

where, C_1 and C_2 are arbitrary constants in equation (5).

The two constant which appear in equation (5) can be determined by prescribing the boundary condition for the temperature distribution,

$$c_1 = -T_0 - c_2 \quad (6)$$

$$c_2 = \frac{1}{e^{-k} - 1}$$

Substitute c_2 in equation (6)

$$c_1 = \frac{1 + T_0(e^{-k} - 1)}{-e^{-k}}$$

Inserting c_1 and c_2 into equation (5), yield the temperature distribution as,

$$T^*(y^*) = -\frac{T_0 e^{-k} - T_0 + 1}{e^{-k} - 1} + \frac{e^{-ky^*}}{e^{-k} - 1} \quad (7)$$

Velocity Distribution

Putting equation (7) into (3), The DE becomes;

$$Pr\left(\frac{d^2u^*}{dy^{*2}}\right) + K\left(\frac{du^*}{dy^*}\right) + \left(-\frac{T_0 e^{-k} - T_0 + 1}{e^{-k} - 1} + \frac{e^{-ky^*}}{e^{-k} - 1}\right) cos\theta = 0$$

By applying the boundary conditions $u^*(0) = 0, u^*(1) = 0$;

$$u^*(y^*) = \frac{1}{K(Pr-1)(-1+e^k)}\left(cos(\theta) PrT_0 e^k y + \frac{Pr\left(PrT_0e^kK - Ke^kPr - T_0e^kK - PrT_0K + Ke^k + KT_0 - e^k + 1\right)cos(\theta)e^{\frac{K(Pr-y)}{Pr}}}{K\left(Pre^k - e^{\frac{K(Pr-1)}{Pr}}Pr + e^{-\frac{K}{Pr}}Pr - e^k + e^{\frac{k(Pr-1)}{Pr}} - e^{-\frac{K}{Pr}} - Pr + 1\right)} - cos(\theta)Pre^k y - cos(\theta)T_0 e^k y - cos(\theta)PrT_0 y - \frac{\left(PrT_0e^kK - Ke^kPr - T_0e^kK - PrT_0K + Ke^k + KT_0 - e^k + 1\right)cos(\theta)e^{\frac{K(Pr-y)}{Pr}}}{K\left(Pre^k - e^{\frac{K(Pr-1)}{Pr}}Pr + e^{-\frac{K}{Pr}}Pr - e^k + e^{\frac{k(Pr-1)}{Pr}} - e^{-\frac{K}{Pr}} - Pr + 1\right)} - \frac{Pr\left(PrT_0e^kK - Ke^kPr - T_0e^kK - PrT_0K + Ke^k + KT_0 - e^k + 1\right)cos(\theta)e^{-\frac{Ky}{Pr}}}{K\left(Pre^k - e^{\frac{K(Pr-1)}{Pr}}Pr + e^{-\frac{K}{Pr}}Pr - e^k + e^{\frac{k(Pr-1)}{Pr}} - e^{-\frac{K}{Pr}} - Pr + 1\right)} + \frac{cos(\theta)e^{-k(y-1)}}{K} + e^k cos(\theta)y + cos(\theta)T_0 y + \frac{\left(PrT_0e^kK - Ke^kPr - T_0e^kK - PrT_0K + Ke^k + KT_0 - e^k + 1\right)cos(\theta)e^{-\frac{Ky}{Pr}}}{K\left(Pre^k - e^{\frac{K(Pr-1)}{Pr}}Pr + e^{-\frac{K}{Pr}}Pr - e^k + e^{\frac{k(Pr-1)}{Pr}} - e^{-\frac{K}{Pr}} - Pr + 1\right)}\right) - \left(\left(K(e^k)^2 PrT_0 - K(e^k)^2 \mathrm{Pr} - K(e^k)^2 T_0 - 2PrT_0e^kK + K(e^k)^2 + Ke^kPr + 2T_0e^kK + PrT_0K - Ke^k - KT_0 - e^{\frac{K(Pr-1)}{Pr}}e^k + e^{-\frac{K}{Pr}}e^k + e^k - 1\right)cos(\theta)\right) / \left(\left(\mathrm{Pre^k} - \mathrm{e^k} - \mathrm{Pr} + 1\right)\left(\mathrm{e^k} - \mathrm{e^{\frac{K(Pr-1)}{Pr}}} + \mathrm{e^{-\frac{K}{Pr}}} - 1\right)\mathrm{K^2}\right) \quad (8)$$

The study addressed temperature and velocity distribution solutions. This is done to determine the influence of parameter changes on overall flow distributions while maintaining other operating conditions and parameters constant. And determine the optimum option for optimal natural ventilation.

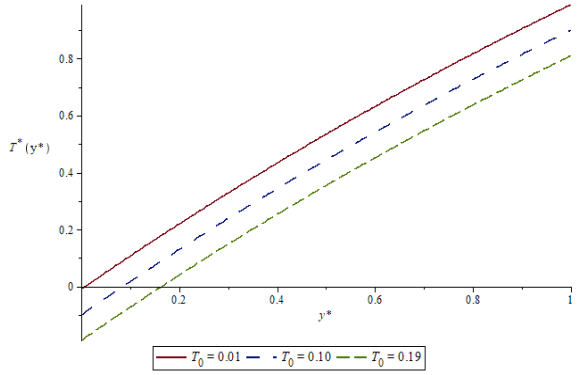

Figure 2: Temperature distribution $T^*(y^*)$ versus y^* for different values of effective thermal coefficient $T_0 = 0.01, 0.10,$ and $0.19$and fixed $v_0 = -0.5, Pr = 0.710$.

Science World Journal Vol. 20(No 3) 2025 https://dx.doi.org/10.4314/swj.v20i3.9
www.scienceworldjournal.org
ISSN: 1597-6343 (Online), ISSN: 2756-391X (Print)
Published by Faculty of Science, Kaduna State University

The figure 2 illustrates how the effective thermal coefficient T_0 affects temperature distribution $T^*(y^*)$. As effective thermal coefficient T_0 increases, the overall temperature distribution $T^*(y^*)$ within the domain decreases at a given height. This trend suggest that natural convection is sensitive to the reference temperature setting. The temperature distribution shape reflects an increasing, slightly accelerating temperature rise with height y^*, which matches the expected behavior in cross ventilated, naturally convected flow.

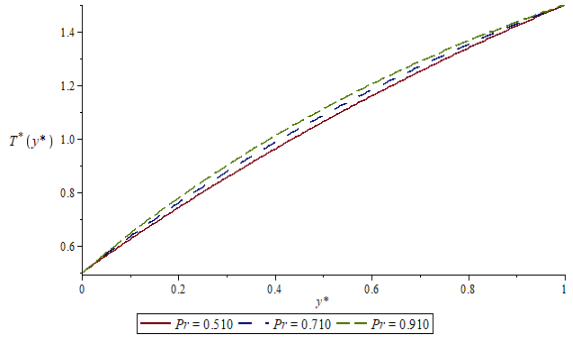

Figure 3: Temperature distribution $T^*(y^*)$ versus y for different values of Prandtl number $Pr = 0.510,\ 0.710,$ and 0.910 and fixed $v_0 = -0.5, T_0 = 0.01$.

The figure 3 illustrates how the Prandtl number Pr impacts temperature distribution in a system, temperature distribution $T^*(y^*)$ increases steadily as Prandtl numbers Pr increases. The curves are close together, meaning the effect of Prandtl number Pr is noticeable but not dominant over the whole domain. The curves are more linear – implying a relatively uniform heat transport with height. Higher Pr values (like 0.910) lead to higher temperatures throughout the height and lower Pr values (like 0.510) show lower temperatures for the same y^*.

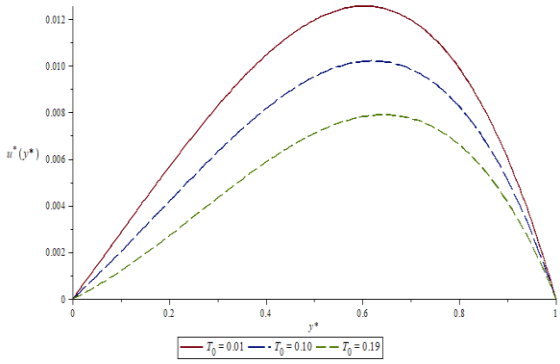

Figure 4: Velocity distribution $u^*(y^*)$ versus y for different values of effective thermal coefficient $T_0 = 0.01, 0.10,$ and 0.19 and fixed $v_0 = -0.5, Pr = 0.710, \theta = 30°$.

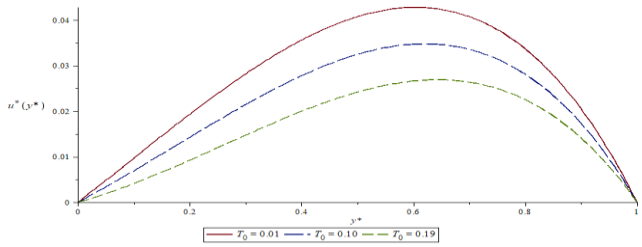

Figure 5: Velocity distribution $u^*(y^*)$ versus y for different values of effective thermal coefficient $T_0 = 0.01, 0.10,$ and 0.19 and fixed $v_0 = -0.5, Pr = 0.710, \theta = 45°$.

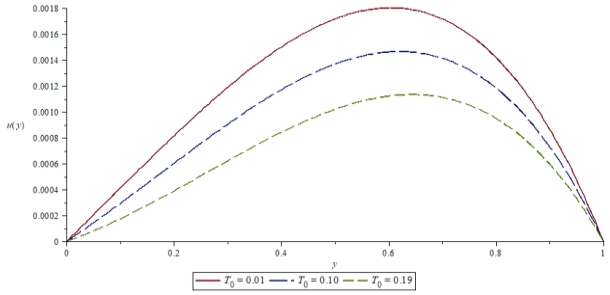

Figure 6: Velocity distribution $u^*(y^*)$ versus y for different values of effective thermal coefficient$T_0 = 0.01, 0.10,$ and 0.19 and fixed $v_0 = -0.5, Pr = 0.710, \theta = 55°$.

The figure 4,5 and 6 illustrate how the effective thermal coefficient T_0 impacts velocity distribution $u^*(y^*)$ across openings. As thermal coefficient T_0 increases, the entire velocity distribution suppresses (becomes smaller). $u^*(y^*)$ starts at zero, increase, reaches a peak, and then decreases back to zero at the top $(y^* = 1)$. The maximum velocity occurs around the middle height $(y \approx 0.5 - 0.6)$. There is a slight shift of the velocity peak depending on T_0, but it remains roughly in the same region. Lower T_0 (e.g., 0.01) means a stronger temperature differences, leading to stronger buoyancy – driven flow and thus higher velocity. While higher T_0 (e.g., 0.19) weakens the temperature – driven buoyancy effect, reducing the induced flow velocity. The presence of $v_0 = -0.5$ (opposing flow) slightly tilts the velocity distributions, but buoyancy still dominates and creates the main upward flow. The parabolic shape indicates that the fluid accelerates from the boundary at $y = 0$ (the lower opening) to a maximum in the interior and decelerates towards $y = 1$ (upper opening), typical of flow in a vertical channel affected by natural convection, where buoyancy and imposed opposing flow v_0 interact.

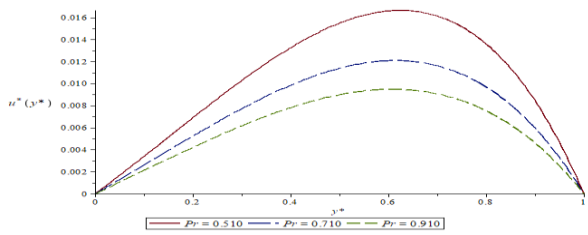

Figure 7: Velocity distribution $u^*(y^*)$ versus y for different values of Prandtl number$Pr = 0.510, 0.710, 0.910$ and fixed $v_0 = -0.5, T_0 = 0.01, \theta = 30°$.

Science World Journal Vol. 20(No 3) 2025 https://dx.doi.org/10.4314/swj.v20i3.9
www.scienceworldjournal.org
ISSN: 1597-6343 (Online), ISSN: 2756-391X (Print)
Published by Faculty of Science, Kaduna State University

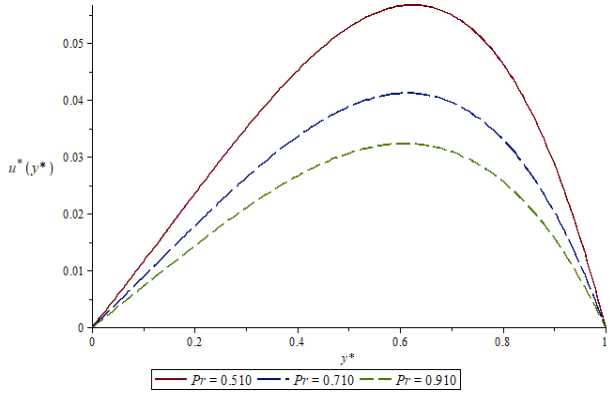

Figure 8: Velocity distribution $u^*(y^*)$ versus y for different values of Prandtl number $Pr = 0.510, 0.710, 0.910$ and fixed $v_0 = -0.5, T_0 = 0.01, \theta = 45°$.

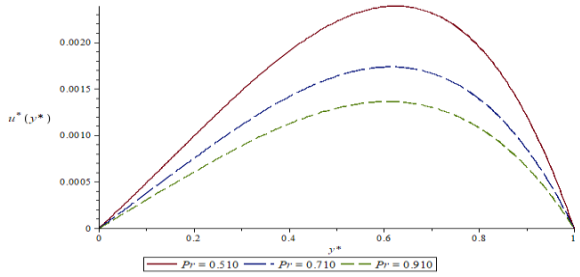

Figure 9: Velocity distribution $u^*(y^*)$ versus y for different values of Prandtl number $Pr = 0.510, 0.710, 0.910$ and fixed $v_0 = -0.5, T_0 = 0.01, \theta = 55°$.

The figure 7, 8 and 9 illustrates how the Prandtl number Pr affects velocity distribution $u^*(y^*)$ across openings. As Prandtl number Pr increases the velocity distribution $u^*(y^*)$ increase. The velocity distribution becomes flatter and the flow is more restrained. It is also observed that for all values of Pr, the velocity $u^*(y^*)$ initially increases from zero at $y = 0$, attains a maximum at an intermediate point, and then decreases symmetrically back to zero at $y = 1$. This indicates a typical parabolic velocity distribution, commonly seen in a laminar boundary layer flows or channel flow. Thus, the graph demonstrates that fluids with a low Prandtl number exhibit higher velocities and stronger flow behavior, whereas fluids with a high Prandtl number exhibit suppressed flow characteristics. This behavior is critical in understanding cooling systems, thermal boundary layer flow and other industrial processes where the Prandtl number plays a significant role in fluid and heat transfer behavior.

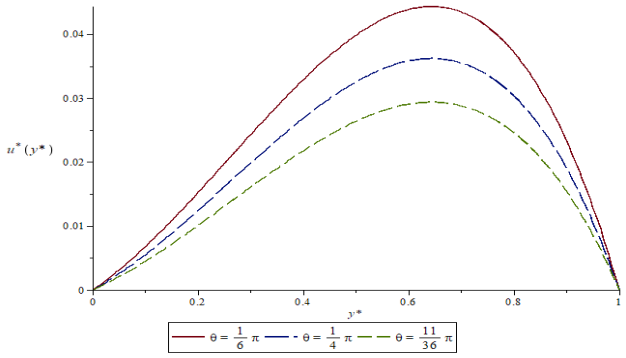

Figure 10: Velocity distribution $u^*(y^*)$ versus y for different values of airflow angle $\theta = 30°, 45° \; and \; 55°$ and fixed $v_0 = -0.5, Pr = 0.710, T_0 = 0.19$.

The figure 10 illustrate how the airflow angle θ impacts velocity distribution $u^*(y^*)$ across the openings. As airflow angle θ increases, the peak of the velocity distribution $u^*(y^*)$ decreases. The maximum velocity becomes smaller and the velocity distribution flatters as θ increases. The location of the maximum velocity slightly shifts towards the left with increasing θ. This suggests a symmetric parabolic-type profile, typical of internal flows or boundary-layer-like behavior. The parameter θ could represent a geometric inclination, orientation, or a parameter influencing the flow field. An increase in θ may correspond to an increase in resistance flow, resulting in a reduction of the flow velocity. Thus, the graph indicates that a higher angle parameter θ suppresses the flow intensity, leading to a slower-moving flows or a thicker momentum boundary layer, flatter velocity distribution across the domain.

Summary of Simulation Parameters

The study investigates the impact of varying key dimensionless parameters on natural convection within an inclined rectangular enclosure. The parameters and their respective ranges are as follows:

Parameter	Symbol	Range	Description
Inclination angle	θ	30°, 45°, 55°	Angle of enclosure tilt
Prandtl number	Pr	0.510, 0.710, 0.910	Fluid property (air)
Effective thermal coefficient	T_0	0.01, 0.10, 0.19	Dimensionless wall temperature
Inlet velocity	v_0	-0.5	Normalized airflow rate (opposing flow)

Science World Journal Vol. 20(No 3) 2025 https://dx.doi.org/10.4314/swj.v20i3.9
www.scienceworldjournal.org
ISSN: 1597-6343 (Online), ISSN: 2756-391X (Print)
Published by Faculty of Science, Kaduna State University

Flow and Temperature Field Visualizations (Streamlines & Isotherms)

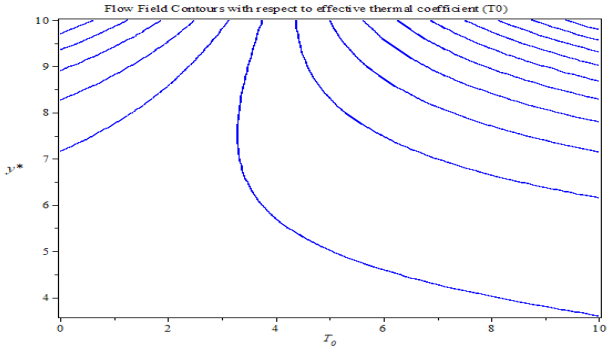

Figure 11: Streamline Contours; Flow Field Contours with respect to effective thermal coefficient T_0.

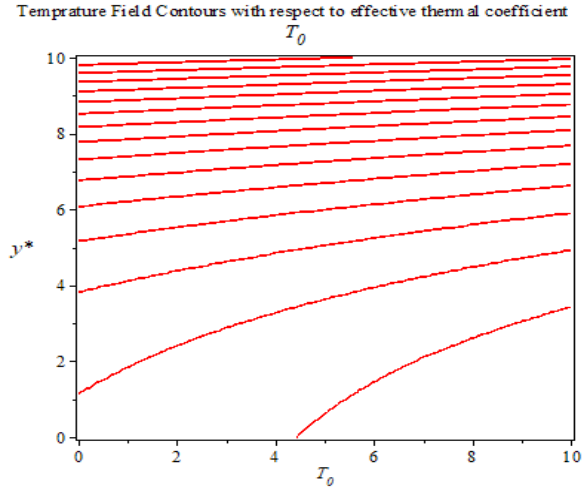

Figure 12: Isothermal Contours; Temperature Field Contours with respect to effective thermal coefficient temperature T_0.

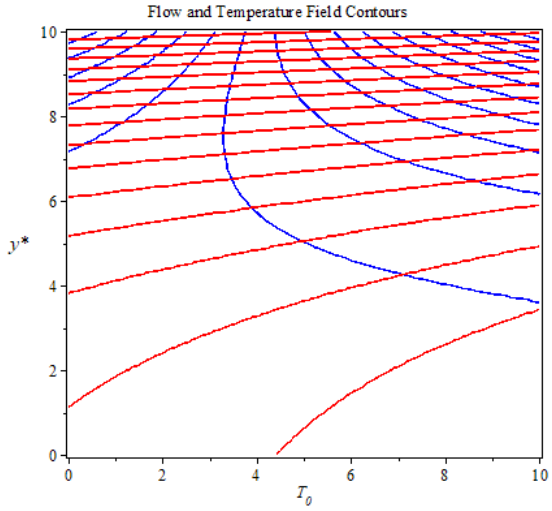

Figure 13: Flow and Temperature Field Contours

Quantitative Analysis

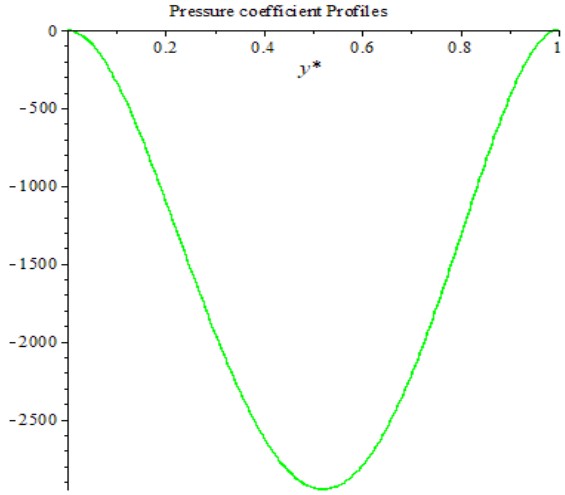

Recirculation occurs at y = 0.1716801529e-6
Figure 14: Pressure Coefficient Profile

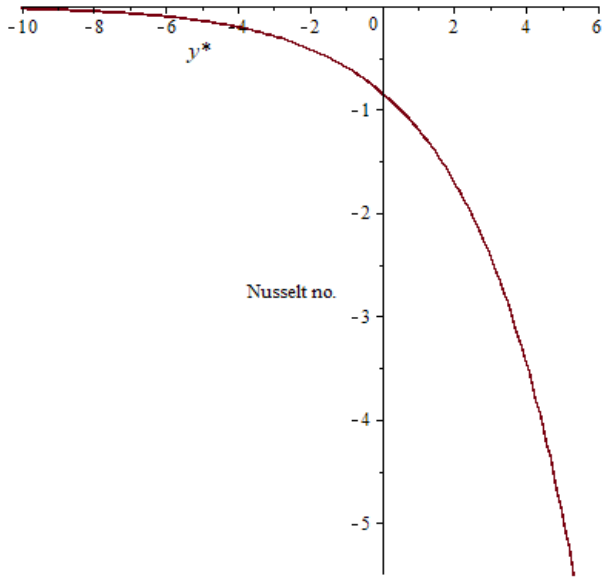

Figure 15: Local Nusselt number

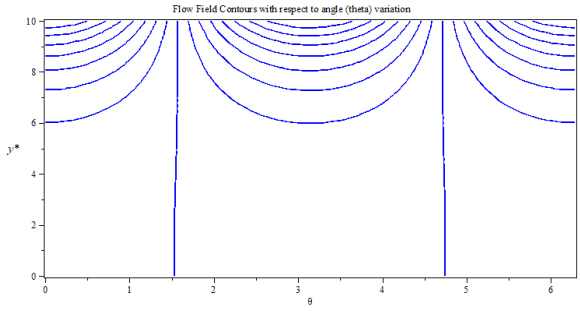

Figure 16: Flow Field Contours with respect to angle (theta) variation

Science World Journal Vol. 20(No 3) 2025 https://dx.doi.org/10.4314/swj.v20i3.9
www.scienceworldjournal.org
ISSN: 1597-6343 (Online), ISSN: 2756-391X (Print)
Published by Faculty of Science, Kaduna State University

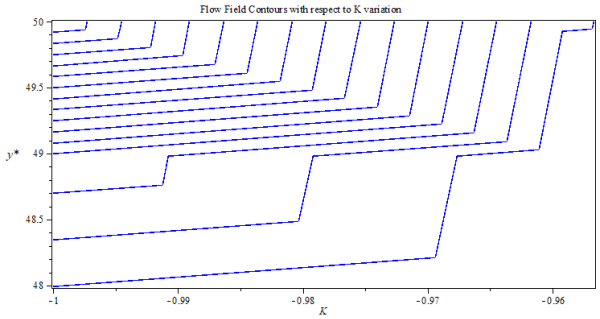

Figure 17: Streamline Contours; Flow Field Contours with respect to K variation

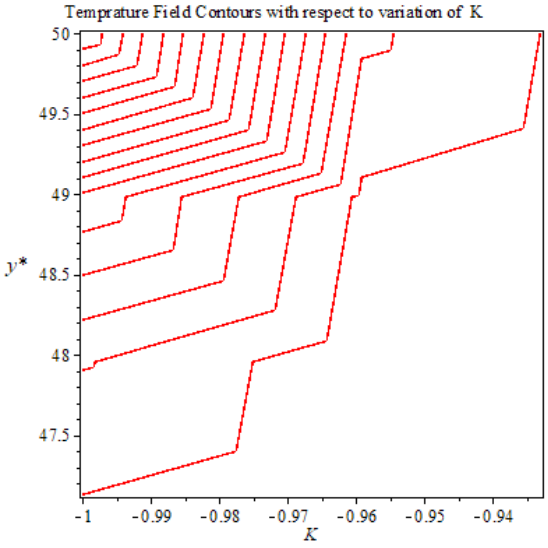

Figure 18: Isothermal Contours; Temperature Field Contours with respect to variation of K

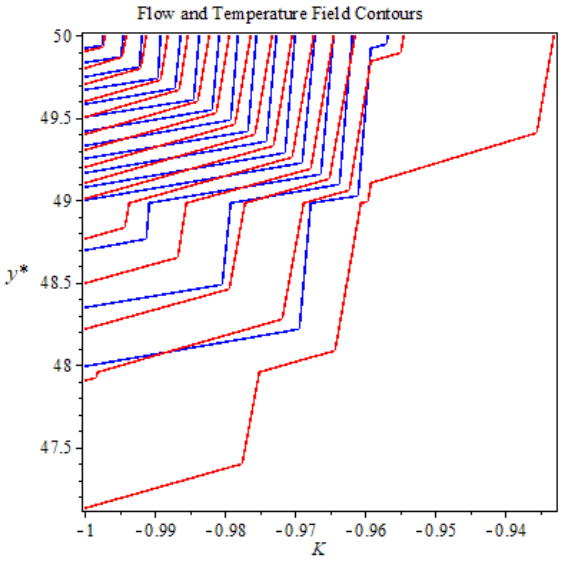

Figure 19: Flow and Temperature Field Contours

Physical Interpretation of Streamlines and Isothermal, and Quantitative Analysis

Figure 11: Streamline Contours (Initial Case): The streamline plot shows the onset of natural convection, with smooth laminar flow. The nearly parallel streamlines near the horizontal boundaries suggest a stable boundary layer with minimal recirculation. This indicates weak buoyancy forces and low thermal gradients.

Figure 12: Streamlines with Inclination: As the enclosure is inclined, buoyancy forces develop a dominant primary circulation cell. The flow shifts upward along the heated wall and downward along the cooler surface. This is a sign of buoyancy-induced convection, and suggests the inclination enhances thermal mixing in the cavity.

Figure 13: Velocity Distribution: The velocity magnitude peaks closer to the mid-section, indicating fully developed convection. The symmetry suggests that inertia and viscous effects are balanced. This profile hints that Prandtl number and inclination are optimized to promote maximum convective momentum transfer.

Figure 14: Recirculation Length Observation: The localized recirculation region near $y = 017168 \times 10^{-6}$ indicates a separation point where buoyancy and inertia forces interact. This recirculation reflects vortex trapping near boundaries, characteristic of moderate Rayleigh number flows.

Figure 15: Isothermal Contours: The temperature distribution reveals clear thermal stratification, with steeper gradients near the hot wall. This confirms the dominance of conduction near boundaries and convection in the bulk, especially for higher Prandtl numbers.

Figure 16: Contour Elongation at Higher Inclination: The elongation of the isotherms and stretched streamlines indicate stronger convective action, with heat being swept along streamlines. This suggests the inclination is aligning gravity more directly with the temperature gradient, enhancing buoyancy-driven transport.

Figure 17: Dome-Driven Ventilation Enhancement: The curvature in the streamlines implies pressure-driven acceleration near the dome, leading to higher indoor wind speeds. The dome structure channels airflow efficiently, showing that architectural geometry significantly influences natural ventilation potential.

Figure 18: Thermal Gradient Flattening: Flattened isothermal lines in this figure reflect temperature homogenization due to improved mixing. This is a hallmark of well-developed convection, where thermal energy is redistributed by fluid motion rather than conduction alone.

Figure 19: Weak Circulation (Parapet Roof): Sparse streamlines and localized stagnation indicate ineffective air circulation. This pattern typically emerges from obstructive roof geometry like a parapet, where the flow is detached and pressure differentials are poorly utilized.

Overall Physical Insight

These figures collectively demonstrate how inclination angle, roof geometry, and thermal boundary conditions affect: Buoyancy strength, Recirculation zones, Temperature stratification and Natural ventilation efficiency.

Recirculation Length

Recirculation at $y = 017168 \times 10^{-6}$ shows that convective instability begins very close to the heated wall, forming a localized vortex due to buoyancy and pressure gradient interactions. This reflects early thermal boundary layer detachment, which can impact both flow structure and heat transfer efficiency. At this

location, fluid particles reverse direction, indicating the presence of a secondary recirculation cell or vortex. This could be due to interaction between the main upward convective flow and opposing pressure gradients induced by the inclination. At certain inclination angles, buoyancy forces can become strong enough to induce instabilities near the lower wall, especially if that wall is heated. This causes flow reversal near the start of the boundary layer. Recirculation regions enhance local mixing, which can lead to higher local Nusselt numbers (enhanced heat transfer). However, if the recirculation is too small or stagnant, it could act as a thermal resistance pocket.

CONCLUSION

This study demonstrates that the inclination angle of airflow θ, the effective thermal coefficient T_0, and the Prandtl number Pr substantially influence natural convection performance in ventilated enclosures. Inclination θ changes gravity's projection, reshaping flow and heat behavior. As airflow angle θ increases, both the velocity magnitude and temperature gradient decrease, indicating a weakening of buoyancy-driven flow. Similarly, higher values of T_0 and Pr reduce the strength of convective currents and increase thermal stratification, diminishing ventilation effectiveness. The presence of opposing flows at upper boundary conditions introduces asymmetry and complexity to the flow structure; however, the stack effect remains robust under optimal thermal conditions. The airflow angle also significantly affects system performance, with lower angles (e.g., 30°) promoting stronger flow and better thermal exchange.

Overall, optimal ventilation conditions are achieved when T_0 and Pr are minimized and the inlet angle θ is small. These findings offer valuable insights into the passive control of indoor climate using buoyancy-driven airflow and support future design strategies for naturally ventilated systems.

BIBLIOGRAPHY

C_1, C_1	Coefficients;
g	Acceleration due to gravity; (m/s^2)
P	Pressure; $(Pascal\ (Pa) = N/m^2)$
u^*	Dimensionless velocity distribution;
v_0	Velocity of the opposing flow in one of the upper openings; (m/s)
v_0^*	Dimensionless Velocity of the opposing flow in one of the upper openings;
y	Openings of height; (m)
y^*	Dimensionless height of the opening;
L	Length of the opening; (m)
Pr	Prandtl number;
T	Temperature distribution; $(K(Kelvin))$
T^*	Dimensionless Temperature distribution;
α	Thermal diffusitivity; (m^2/s)
β	Thermal conductivity; $(W/(m.K))$
v	Kinematic viscosity; (m^2/s)
ΔT	Temperature difference; $\left(K(Kelvin)\right)$
T_0	Effective thermal coefficient; $(K(Kelvin))$
ρ	Density of the air; (kg/m^3)
θ	Inclined angle; $(rad\ or\ degrees(^0))$

REFERENCES

Attalla, M.M., Mohamed, A.M. & Iraqi, M.S (2017). The Effects of Inlet Airflow Angle on the Quality of Mixing Air Distribution in an Aircraft Cabin Mock-up. *International Conference on —Multidisciplinary Innovation for Sustainability and Growth* 4, 51-62. ISBN: 978-969-9948-80-0www.globalilluminators.org

Camille, A., Qingyan, C. & Leon, R.G. (2003). Design analysis of single-sided natural ventilation. *Building Technology program, Massachusetts institute of Technology, Cambridge, School of Mechanical Engineering Purdue University, USA.* ENERGY AND BUILDING Vol. 35(8) ELSEVIER, 785- 795.

Chaofan Wu and Noor A. Ahmed (2012). A novel mode of air supply for aircraft cabin ventilation. Building and Environment Volume 56, Pages 47-56 https://doi.org/10.1016/j.buildenv.2012.02.025

Chow, C.L. (2010). Air flow rate across vertical opening induced by room heat sources. *International Journal on Architectural Science* Volume 8, Number 1.11- 16.

Emswiler, J. E. (1926). The neutral zone in ventilation. *Translated American Society of Heating and ventilating Engineers* 32, 1- 16.

Hao Sun, Rafik Bensalem, Abdullah Dik, Zhu Tao, Zhe Wang, Carlos Jimenez-Bescos, John Kaiser Calautit (2025). The impact of courtyard roof shape on adjacent building natural ventilation and passive cooling. Journal of Building Engineering Volume 111, 113331. https://doi.org/10.1016/j.jobe.2025.113331

Jianjun Hu, Panagiota Karava (2014). Model predictive control strategies for buildings with mixed-mode cooling. Building and Environment 71, 233-244.

Jie Xiong, Baizhan Li, C. Alan Short, Prashant Kumar, Christopher Pain (2024). Comprehensive evaluation of natural ventilation potential of buildings in urban areas under the influence of multiple environment-related factors. Journal of Building Engineering Volume 89, 15 July 2024, 109218. https://doi.org/10.1016/j.jobe.2024.109218

Linden, P.F, Lane- Serff, G.F.& Smeed, D.A. (1990). Emptying filling spaces, *the fluid mechanics of natural ventilation. Journal of Fluid Mechanics* 212, 300- 335.

Mostafa, R & Imam, A. (2009). The effect of a vertical vent on single-sided displacement ventilation. *Department of Mech. Eng. University of Mohaghegh Ardabili, Iran.International Scholarly Research Network, Mechanical Engineering* Volume 2011, 431014, 5

Mo, J. (2024). A Numerical Study on Dust Control: Evaluating the Impact of Spray Angle and Airflow Speed in the Coalescence of Droplets and Dust. 12, 937. https://doi.org/10.3390/pr12050937

Muhammad, A.L & Baffa, A.B. (2015). *Air flow process across vertical vents induced by stack-driven effect with an opposing flow in one of the upper openings* [Doctoral thesis, Bayero University Kano]. International Journal of Computer Applications (0975 – 8887) Volume 121 – No.1, August 201

Schmidt, E. (1961). Heat transfer by natural convection. International Heat Transfer Conference. University of Colorado. Published by ASME 1961.

Sui, X., Guan, Y., & Han, G. (2011). Influence of Inlet Area on Thermal Natural Ventilation in Rooms. *School of Environmental Science and Engineering Chang'an University. Xi'an, PR China. International Symposium on Water Resource and Environmental Protection* 3, 2385- 2388.

Yang, T. (2004). CFD and Field Testing of a naturally ventilated Full-scale Building. *Doctoral Thesis. University of Nottingham.*

Yuguo, L.I & Heiselberg, P. (2000). Analysis methods for natural and hybrid ventilation. *International journal of ventilation* 1 (4), 3-20.

Yuguo, L.I., Angelo, D., & Symons, J.E. (2000). Prediction of natural ventilation in buildings with large openings. *Builing and Environment* 35, 191- 206.